THE JOURNAL OF PHYSICAL CHEMISTRY Letters

Letter

pubs.acs.org/JPCL

Spectral Contributions to the Thermal Conductivity of C_{60} and the Fullerene Derivative PCBM

Ashutosh Giri* and Patrick E. Hopkins*

Department of Mechanical and Aerospace Engineering, University of Virginia, Charlottesville, Virginia 22904, United States

ABSTRACT: We investigate the heat transport mechanisms responsible in driving the characteristic temperature-dependent thermal conductivities of C_{60} and PCBM crystals via molecular dynamics simulations. We find that the thermal conductivity of PCBM is "ultralow" across the temperature range studied in this work. In contrast, the temperature-dependent thermal conductivity of C_{60} crystals exhibits two regimes: "crystal-like" behavior at low temperatures where thermal conductivity increases rapidly with decreasing temperature and temperature-independent thermal conductivities at higher temperatures. The spectral contributions to thermal conductivity for C_{60} suggest that the majority of heat is carried by modes in the low-frequency regime (<2 THz), which is a consequence of intermolecular interactions. Unlike for C_{60}, these modes are not responsible for heat conduction in PCBM due to the mismatch in density of states introduced by the addition of low-frequency modes from the alkyl chains that are attached to the fullerene moieties.

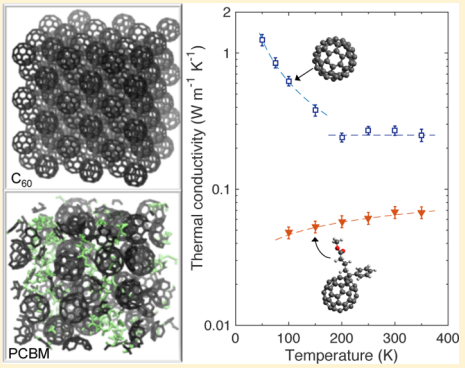

The capability of fabricating carbon nanostructures (e.g., C_{60}) in macroscopic quantities[1,2] has triggered their use in a plethora of applications such as photovoltaics,[3,4] thermoelectrics,[5,6] and phase change memory devices.[7] Common to these applications, the management of heat and thermal characterization in fullerenes and their derivatives is critical for their commercialization. For example, the complete understanding of thermal transport has significance in properly accounting for Joule heating in photovoltaic and phase change memory devices,[7−9] and likewise, knowledge of heat transport mechanisms is necessary for thermoelectric applications where materials with ultralow thermal conductivities and high electron mobilities are desirable.[6,10]

Considering the impact that thermal characterization of C_{60}-based materials has on their device-driven applications, relatively few studies have focused on investigating their thermal properties. In this context, it has been shown that bulk C_{60} crystals demonstrate low thermal conductivities, ∼0.4 W m^{-1} K^{-1} measured via the static one-heater, two-thermometer method and the 3ω technique.[11,12] Moreover, the temperature dependence of the thermal conductivity revealed an abrupt jump at 260 K as a result of an orientational-order transition in C_{60} crystals. Similarly, molecular dynamics (MD) simulations have revealed that at temperatures greater than 200 K C_{60} molecules rotate unhindered at high frequencies, whereas at lower temperatures, orientational freezing is observed.[13,14]

The attachment of alkyl chains, or other such moieties, on the fullerene (as in the case of the semiconducting PCBM, [6,6]-phenyl C_{61}-butyric acid methyl ester) can have a significant change in structural and physical properties,[15,16] including alteration of the characteristic thermal transport mechanisms driving their thermal conductivities. Experimental investigations of thermal properties of fullerenes and their derivatives have revealed almost an order of magnitude difference between the thermal conductivities of hexagonal PCBM and face-centered cubic C_{60}.[17−21] Using time domain thermoreflectance, Duda et al.[17,18] reported ultralow thermal conductivities (0.03−0.06 W m^{-1} K^{-1} at room temperature) for PCBM, which marked the lowest ever measured thermal conductivity for fully dense solids. They attributed the reduced thermal conductivity to vibrational scattering resulting from the addition of molecular moieties on the fullerene molecules. Recently, Chen et al.[22] performed nonequilibrium molecular dynamics (NEMD) simulations on PCBM at 300 K and ascribed the reason for the ∼63% decrease in thermal conductivity (from the addition of the molecular tails) to localization of vibrational states and reduced group velocities of heat carrying vibrations in PCBM as compared to bare C_{60} structures. They also demonstrated that the mismatch of the vibrational density of states (DOS) between the alkyl chain and the fullerene could potentially result in the scattering of low-frequency vibrations. However, a thorough understanding of thermal transport, which includes the mode-level details of the amount of heat carried by different frequencies and the characteristic temperature dependence of thermal conductivities in C_{60} and PCBM, is still lacking. In particular, the important questions that need to be addressed to gain more insight into the thermal transport properties of fullerenes and their derivatives are (i) what frequencies carry heat in the C_{60} crystal and how do these spectral contributions differ with the addition of the alkyl chain on the fullerene moiety and (ii) how

Received: March 12, 2017
Accepted: April 25, 2017
Published: April 25, 2017

DOI: 10.1021/acs.jpclett.7b00609
J. Phys. Chem. Lett. 2017, 8, 2153−2157

does orientational freezing affect the vibrational properties and the MD-predicted temperature-dependent thermal conductivity of fcc C_{60}. In this Letter, we seek to answer these questions by performing MD simulations on model C_{60} and PCBM crystals.

We perform the MD simulations using the LAMMPS package with a time step of 1 fs for all simulations.[23] Consistent with Chen et al.'s[22] prior study of thermal properties of C_{60} and PCBM, we implement the polymer consistent force field (PCFF) to describe the inter- and intra-atomic interactions, which include van der Waals forces, bond angles, dihedrals, and improper interactions.[24,25] Initially, fullerene molecules are placed in a fcc lattice with a center-to-center distance between the molecules of 9 Å.[26] Similarly, the PCBM molecules are placed in their respective hexagonal lattices. The structures are allowed to relax under *NPT* integration, which is the isothermal−isobaric ensemble with the number of particles, pressure, and temperature of the system held constant for a total of 1 ns at 0 bar of pressure. Following *NPT* integration, we also perform *NVT* integration (which is the Nose−Hoover thermostat[27] with the number of atoms, volume, and temperature of the simulation held constant) at the prescribed temperature for another 1 ns. After equilibration, the densities of the C_{60} and PCBM structures are 1.75 and 1.48 g cm^{-3}, respectively, at room temperature. The experimentally determined densities of C_{60} and PCBM are 1.68 and 1.52−1.61 g cm^{-3}, respectively, which are in good agreement with the densities of our simulated structures.[21] An equilibrated computational domain for the 55 × 55 × 55 Å^3 periodic fcc structure of the C_{60} crystal is shown in Figure 1a.

To efficiently calculate the thermal conductivities of our simulated C_{60} and PCBM, we implement the Green−Kubo (GK) and NEMD approaches for the C_{60} and PCBM structures. The reason for implementing two different approaches is to gauge the computational efficiency of the two methods and to gain comparable levels of precision on the thermal conductivities reported for the two different computational domains.[28] We note that we have conducted both GK and NEMD simulations on all structures and conclude that due to considerable size effects in the C_{60} (a consequence of long mean-free-path vibrations carrying most of the heat),[29] the GK approach can be implemented to obtain thermal conductivities with high precision. For PCBM, no size effects are observed for structures with simulation domain lengths greater than ∼20 nm. Note that the GK and NEMD approaches predict comparable thermal conductivities for PCBM. However, due to comparatively lower uncertainty in the NEMD results, we report the NEMD-predicted values for our PCBM; similar NEMD results at room temperature were obtained by Chen et al.,[22] where the authors demonstrate the prevalence of size effects in C_{60} and the absence of size effects in PCBM.

Figure 1a shows the relaxed C_{60} computational domain used to predict the thermal conductivity. Note that the 55 × 55 × 55 Å^3 periodic system with 15 360 atoms used in this work is large enough to eradicate any size effects in the GK predictions for the C_{60} structures. Figure 1b−d shows the converged values of thermal conductivities at three characteristic temperatures, which are obtained from the respective integrals of the heat current autocorrelation functions (HCACFs) shown in the insets.[30,31] As shown in Figure 1b−d, a total time of ∼80 ps is enough to record a converged value of the HCACF, and the thermal conductivity is determined from the procedure outlined in ref 31. For the NEMD approach, we calculate the temperature profiles under a microcanonical ensemble with the

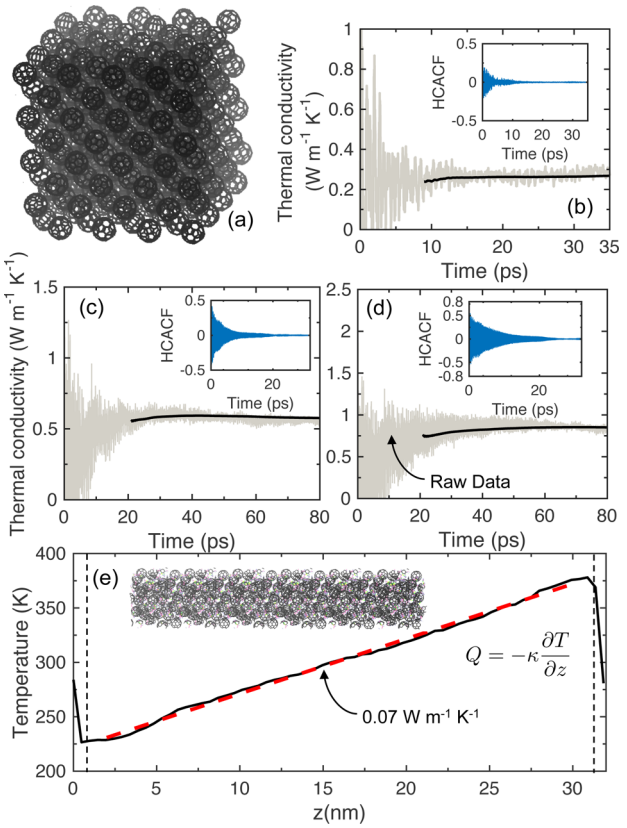

Figure 1. (a) Schematic of the 55 × 55 × 55 Å^3 periodic computational domain used for Green−Kubo (GK) calculations for C_{60}. Converged values of the thermal conductivities obtained from the integrals of the HCACFs (shown in the inset) for C_{60} at (b) 300, (c) 100, and (d) 75 K. (e) Time-averaged steady-state temperature profile for the PCBM structure (schematic of the computational domain shown in the inset) at room temperature.

number of particles, volume, and energy held constant. The steady-state temperature profiles are obtained by applying a fixed amount of energy per time step to a warm bath at one end and removing the equal amount of energy from a cool bath at the other end. After 5 ns of adding and removing heat from the heat baths, the steady-state temperature profile thus obtained is used to predict the thermal conductivity by invoking the Fourier law, $Q = -\kappa \partial T/\partial z$, where the applied flux, Q, is in the z-direction. An example of the temperature profile for the PCBM structure (see the inset of Figure 1c) at room temperature is shown in Figure 1c. For all reported values of thermal conductivity, the uncertainty is determined from five simulations with different initial conditions.

The MD-predicted thermal conductivities for our C_{60} and PCBM crystals are shown in Figure 2. The temperature dependence of thermal conductivity for the PCBM (or lack thereof) is similar to the experimentally reported temperature dependence by Duda et al.[17,18] The thermal conductivity of PCBM at room temperature is also consistent with the NEMD predictions by Chen et al.[22] and agrees very well with the experimentally measured values.[18,19] We note that, while the PCBM molecules are placed in a hexagonal lattice in this work, the alkyl chains are not oriented in the same direction. However, as our MD predictions of thermal conductivity for PCBM agree well with those reported by Chen et al.[22] with the alkyl chains oriented in the same direction, the disorder in the PCBM most likely does not further lower the thermal

DOI: 10.1021/acs.jpclett.7b00609
J. Phys. Chem. Lett. 2017, 8, 2153−2157

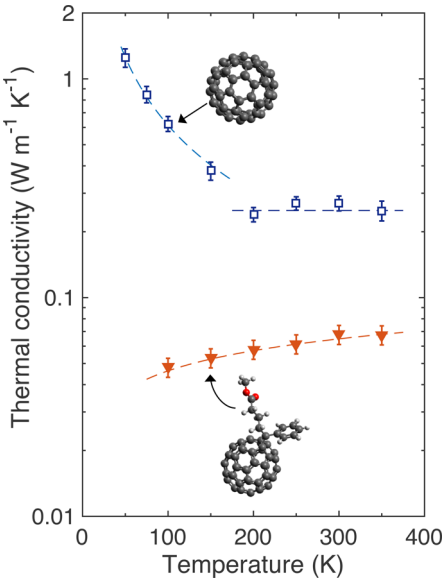

Figure 2. Temperature-dependent thermal conductivity predictions from the GK approach for C_{60} and the nonequilibrium MD approach for PCBM structures. The thermal conductivity of PCBM demonstrates amorphous behavior, whereas for the C_{60} crystal, a jump in thermal conductivity below 200 K marks the transition from "crystal-like" to temperature-independent thermal transport behavior. The dashed lines are to guide the eye.

conductivity of these structures as predicted via MD simulations.

In contrast to the MD-predicted thermal conductivity of PCBM, our results for C_{60} crystals do not agree with the experimentally reported values in the literature.[11,12] Yet, the 0.27 ± 0.025 W m^{-1} K^{-1} calculated via the GK approach at room temperature is consistent with the prior NEMD results from Chen et al.[22] This discrepancy with experimental results has been attributed to the error introduced due to the linear fitting in a relatively small range of system sizes considered in their NEMD simulations.[22] While this could potentially lead to lower predictions of thermal conductivity, our GK results are also ∼33% lower than the experimentally reported values, which suggests that size effects are not likely the cause of the discrepancy. We note that the PCFF potential used to describe the interatomic interactions might potentially not be sufficient to reproduce the absolute values of the experimentally measured thermal conductivities. Furthermore, the velocities of atoms in our classical MD simulations are described by the Maxwell−Boltzmann distribution, where the entire vibrational spectrum of the system is excited at all temperatures. This classical nature of the simulations could also be one of the reasons for the discrepancy between the MD-predicted thermal conductivities and the experimental results. However, for the various reasons that we discuss later in this Letter regarding the low-frequency mode contributions, we do not expect the relative trends and differences in thermal conductivities among the two systems studied in this work to change.

For the C_{60} crystals, even though the MD predictions do not quantitatively match with the experimentally determined values, similar temperature trends are observed. Most notably, the abrupt jump in thermal conductivity below ∼200 K is qualitatively similar to that observed in experiments conducted by Yu et al.[11] where the jump is observed at 260 K. They attributed the sharp jump to the strong scattering of phonons in the orientationally disordered fcc phase, leading to temperature-independent thermal conductivity above 260 K. The "crystal-like" thermal conductivity behavior below 260 K has been attributed to orientational freezing;[32] similar behavior has also recently been reported for binary superatomic crystals of $Co_6Se_8(PEt_3)_6(C_{60})_2$ in ref 32.

To gain more insight into the intrinsic vibrational properties and spectral contributions to thermal conductivity of the C_{60} and PCBM structures, we calculate the DOS and implement the spectral analysis method as described in our previous work (ref 33). Briefly, for the spectral analysis, the heat current between atoms i and j is proportional to the correlation of the interatomic force $\vec{F}_{ij}$ between the atoms and the velocities, $q_{i\to j}(\omega) \propto \langle \vec{F}_{ij}\cdot(\vec{v}_i + \vec{v}_j)\rangle$, where the brackets denote a steady-state nonequilibrium ensemble average.[33−36] To calculate the spectrally resolved thermal conductivities, forces and velocities for the atoms under consideration are tabulated for a total of 10 ns with 10 fs time intervals under *NVE* integration. Similarly, the DOS is calculated by taking the Fourier transform of the velocity autocorrelation function.[37]

Figure 3a shows the bulk DOS for the two structures. The molecular tails in the PCBM broaden the sharp peaks seen in the vibrational spectra of the C_{60} crystal and also shift them to lower frequencies. This is expected as the molecular tails increase the length and mass of the molecules, which manifests in the vibrational spectrum by adding low-frequency modes, while the stiffer interatomic interactions between the sp^3 carbon and the lighter atoms (or the C−H stretching modes) only slightly increase the higher-energy spectrum of the crystals.

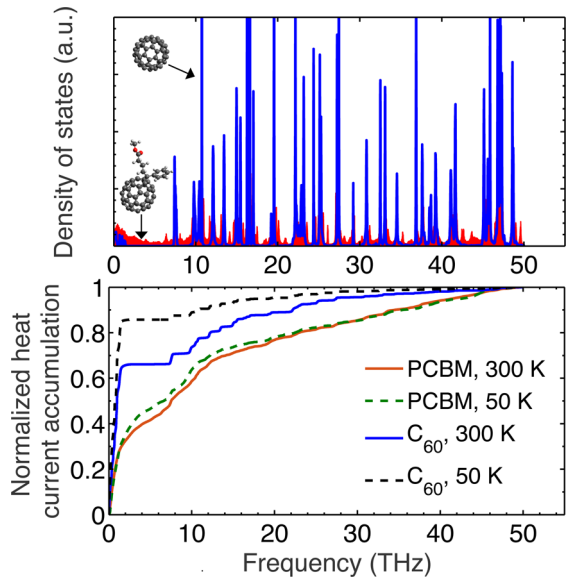

Figure 3. (a) Vibrational DOS for the C_{60} and PCBM structures. (b) Normalized heat current accumulation for the two structures at high (300 K) and low (50 K) temperatures.

Figure 3b shows the normalized heat current accumulation for our C_{60} and PCBM crystals at high (300 K) and low (50 K) temperatures. At high temperatures for the C_{60} domains, the thermal conductivity is dominated by the zone center modes that are associated with long wavelength (frequencies lower than 3 THz). In fact, ∼65% of the heat is carried by vibrations of <3 THz. The intramolecular C−C stretching modes also contribute ∼30% to the thermal conductivity of C_{60} at the high temperature. In comparison to the case of C_{60}, frequencies of

DOI: 10.1021/acs.jpclett.7b00609
J. Phys. Chem. Lett. 2017, 8, 2153−2157

<3 THz do not contribute significantly to the thermal conductivity of PCBM, and a significant amount of heat is carried by vibrations in the 3−10 THz range (on a per-mode basis). This reduced contribution to the thermal conductivity in the <3 THz range in the PCBM as compared to that in the C_{60} could potentially be the result of scattering (due to the DOS mismatch) between the very low frequencies that are less than 3 THz (intrinsic to the C_{60} intermolecular vibrations) and the modes in the 3−10 THz range added due to the alkyl chains.[22] Furthermore, it is also noteworthy that the higher-frequency regime (>20 THz) contributes ∼25% to the total thermal conductivity in PCBM, whereas they have negligible influence on heat flow in the C_{60} crystal. Note, that as MD simulations are strictly classical in nature, all of the available vibrational modes as shown in Figure 3a are activated.

Figure 3b also shows the spectral contributions at a characteristic low temperature where the thermal conductivity of C_{60} demonstrates an Umklapp scattering-dominated $1/T$ temperature trend. For the C_{60} crystals, in comparison to the high-temperature contributions to thermal conductivity, the low-temperature contributions of vibrations in the <3 THz range increase notably. This can be related to the "orientational freezing" of rotational modes at low temperatures that results in a lower scattering of the intermolecular modes, as we discuss in more detail below. However, for the PCBM structures, the spectral contributions at high and low temperatures are similar, which is consistent with the temperature-independent thermal conductivities predicted by our MD simulations.

The spectral contributions presented in Figure 3b can be directly correlated to the harmonic lattice dynamics calculations of the phonon dispersion relations conducted by Chen et al.[22] for C_{60} and PCBM structures. Specifically, for C_{60}, vibrational frequencies of <2 THz have considerably higher group velocities, $|v_g = \partial\omega/\partial k|$, and therefore larger contributions to the thermal conductivity. However, for PCBM, the group velocities are high for phonons with $f < 1$ THz, while the remainder of the spectrum demonstrates very low group velocities with flat dispersion curves. As noted earlier, while PCBM has modes in the 3−10 THz frequency range that contribute to thermal transport, this frequency range is unoccupied for the C_{60} crystal (as is evident from the DOS in Figure 3a and from the phonon dispersion curves in ref 22), which manifests in the heat flux accumulation with zero contribution to the thermal conductivity for this frequency range (cf. Figure 3b).

Finally, we turn our focus to the modes that carry the most significant amount of thermal energy in the C_{60} crystals. Figure 4 shows the DOS in the low-frequency region for the C_{60} under different conditions. In Figure 4a, the low-frequency regime is shown for a computational domain where the angular momentum of the buckyballs is set to zero every time step after equilibration. In other words, we restrict the freely rotating motion of the buckyballs during the simulations. This allows us to separate the contributions from the rotational motion to the DOS of C_{60}. It is clear from Figure 4a that the effect of hindering the rotation is mainly observed in the near-zero part of the frequency spectrum where the DOS is considerably diminished (see Figure 4a). This suggests that the low-frequency peak in the DOS for the C_{60} can be attributed to the collective rotational motion of the buckyballs. As noted earlier, at low temperatures (below 200 K for our buckyballs) where the kinetic energy of the C_{60} molecules is not high enough to overcome the energy barrier between the local energy minima,

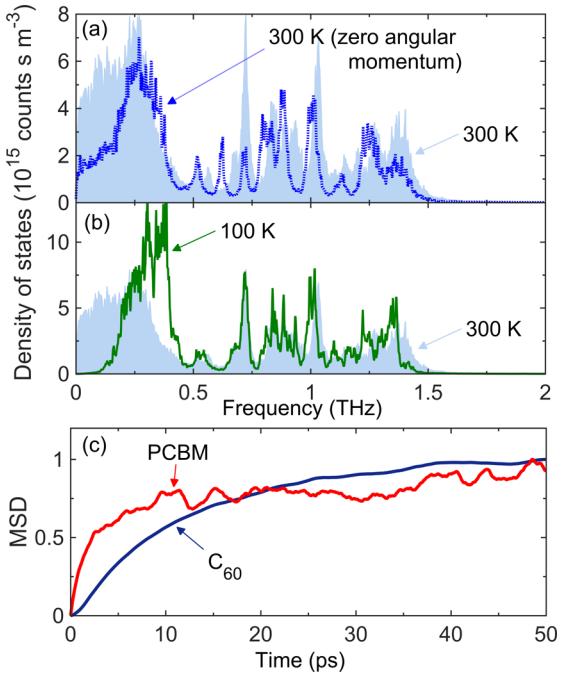

Figure 4. Vibrational DOS in the low-frequency regime (a) at 300 K for C_{60} showing the near-zero peak, which is a result of the rotational motion of the buckyballs. Also included is the DOS when the angular momentum of the buckyballs is set to zero (blue dotted line). (b) DOS at 100 K (solid green line), showing the shift in the low-frequency peak due to orientational freezing. (c) Normalized MSD of the atoms as a function of time between the PCBM and the C_{60} structures.

the rotational degrees of freedom for the buckyballs are "frozen-out". This is clearly seen in Figure 4b, where the low-frequency peak observed at room temperature is shifted to higher frequencies at 100 K.

To quantitatively demonstrate that the low-frequency modes at high temperatures are related to the rotational motion of the C_{60} molecules, we compare the normalized mean-square displacement (MSD) of the atoms as a function of time between the PCBM and the C_{60} structures, which describes their random motion (cf. Figure 4c). For the PCBM, along with an order of magnitude smaller value for the maximum MSD, the MSD converges to a maximum value much faster as compared to that of the C_{60}. As reported by Chen et al.,[22] the time constant related to the slow rise in the MSD for the C_{60} is associated with the ∼0.1 THz peak in the DOS, suggesting that indeed the rotational motion of C_{60} at high temperatures is due to the near-zero frequency modes.

In summary, we have shown that the temperature-dependent thermal conductivity of C_{60} exhibits two regimes: (i) thermal conductivity increases rapidly with decreasing temperature at low temperatures, which is attributed to orientational freezing, and (ii) thermal conductivity is independent of temperature at higher temperatures where diffusive rotational motion results in low thermal conductivity. The calculations of spectral contributions to thermal conductivity reveal that for C_{60} the majority of the heat is carried by modes in the lower-frequency spectrum that result from intermolecular interactions. However, these modes are not responsible for heat conduction in PCBM due to the mismatch in DOS introduced by the addition of low-frequency modes from the molecular tail attached to the fullerene.

DOI: 10.1021/acs.jpclett.7b00609
J. Phys. Chem. Lett. 2017, 8, 2153−2157

AUTHOR INFORMATION

Corresponding Authors

*E-mail: ag4ar@virginia.edu (A.G.).
*E-mail: phopkins@virginia.edu (P.E.H.).

ORCID

Ashutosh Giri: 0000-0002-8899-4964

Notes

The authors declare no competing financial interest.

ACKNOWLEDGMENTS

We would like to thank the Army Research Office for support (Grant No. W911NF-16-1-0320).

REFERENCES

(1) Kroto, H. Space, Stars, C_{60}, and Soot. *Science* **1988**, *242*, 1139−1145.
(2) Kratschmer, W.; Lamb, L. D.; Fostiropoulos, K.; Huffman, D. R. Solid C_{60}: A New Form of Carbon. *Nature* **1990**, *347*, 354−358.
(3) Blom, P.; Mihailetchi, V.; Koster, L.; Markov, D. Device Physics of Polymer:Fullerene Bulk Heterojunction Solar Cells. *Adv. Mater.* **2007**, *19*, 1551−1566.
(4) Saran, R.; Stolojan, V.; Curry, R. J. Ultrahigh Performance C_{60} Nanorod Large Area Flexible Photoconductor Devices via Ultralow Organic and Inorganic Photodoping. *Sci. Rep.* **2015**, *4*, 5041.
(5) Sumino, M.; Harada, K.; Ikeda, M.; Tanaka, S.; Miyazaki, K.; Adachi, C. Thermoelectric Properties of n-type C_{60} Thin Films and Their Application in Organic Thermovoltaic Devices. *Appl. Phys. Lett.* **2011**, *99*, 093308.
(6) Zhang, K.; Zhang, Y.; Wang, S. Enhancing Thermoelectric Properties of Organic Composites through Hierarchical Nanostructures. *Sci. Rep.* **2013**, *3*, 3448.
(7) Kim, C.; Suh, D.-S.; Kim, K. H. P.; Kang, Y.-S.; Lee, T.-Y.; Khang, Y.; Cahill, D. G. Fullerene Thermal Insulation for Phase Change Memory. *Appl. Phys. Lett.* **2008**, *92*, 013109.
(8) Bull, T. A.; Pingree, L. S. C.; Jenekhe, S. A.; Ginger, D. S.; Luscombe, C. K. The Role of Mesoscopic PCBM Crystallites in Solvent Vapor Annealed Copolymer Solar Cells. *ACS Nano* **2009**, *3*, 627−636.
(9) Li, G.; Shrotriya, V.; Yao, Y.; Yang, Y. Investigation of Annealing Effects and Film Thickness Dependence of Polymer Solar Cells Based on Poly(3-Hexylthiophene). *J. Appl. Phys.* **2005**, *98*, 043704.
(10) Dresselhaus, M.; Chen, G.; Tang, M.; Yang, R.; Lee, H.; Wang, D.; Ren, Z.; Fleurial, J.-P.; Gogna, P. New Directions for Low-Dimensional Thermoelectric Materials. *Adv. Mater.* **2007**, *19*, 1043−1053.
(11) Yu, R. C.; Tea, N.; Salamon, M. B.; Lorents, D.; Malhotra, R. Thermal Conductivity of Single Crystal C_{60}. *Phys. Rev. Lett.* **1992**, *68*, 2050−2053.
(12) Olson, J. R.; Topp, K. A.; Pohl, R. O. Specific Heat and Thermal Conductivity of Solid Fullerenes. *Science* **1993**, *259*, 1145−1148.
(13) Cheng, A.; Klein, M. L. Molecular Dynamics Simulations of Solid Buckminsterfullerenes. *J. Phys. Chem.* **1991**, *95*, 6750−6751.
(14) Cheng, A.; Klein, M. L. Molecular-Dynamics Investigation of Orientational Freezing in Solid C_{60}. *Phys. Rev. B: Condens. Matter Mater. Phys.* **1992**, *45*, 1889−1895.
(15) Zheng, L.; Han, Y. Solvated Crystals Based on [6,6]-Phenyl-C_{61}-butyric Acid Methyl Ester (PCBM) with the Hexagonal Structure and Their Phase Transformation. *J. Phys. Chem. B* **2012**, *116*, 1598−1604.
(16) Choi, S.-H.; Liman, C. D.; Krämer, S.; Chabinyc, M. L.; Kramer, E. J. Crystalline Polymorphs of [6,6]-Phenyl-C_{61}-butyric Acid n-Butyl Ester (PCBNB). *J. Phys. Chem. B* **2012**, *116*, 13568−13574.
(17) Duda, J. C.; Hopkins, P. E.; Shen, Y.; Gupta, M. C. Exceptionally Low Thermal Conductivities of Films of the Fullerene Derivative PCBM. *Phys. Rev. Lett.* **2013**, *110*, 015902.
(18) Duda, J. C.; Hopkins, P. E.; Shen, Y.; Gupta, M. C. Thermal Transport in Organic Semiconducting Polymers. *Appl. Phys. Lett.* **2013**, *102*, 251912.
(19) Wang, X.; Liman, C. D.; Treat, N. D.; Chabinyc, M. L.; Cahill, D. G. Ultralow Thermal Conductivity of Fullerene Derivatives. *Phys. Rev. B: Condens. Matter Mater. Phys.* **2013**, *88*, 075310.
(20) Xie, X.; Yang, K.; Li, D.; Tsai, T.-H.; Shin, J.; Braun, P. V.; Cahill, D. G. High and Low Thermal Conductivity of Amorphous Macromolecules. *Phys. Rev. B: Condens. Matter Mater. Phys.* **2017**, *95*, 035406.
(21) Pohls, J.-H.; Johnson, M. B.; White, M. A. Origins of Ultralow Thermal Conductivity in Bulk [6,6]-Phenyl-C_{61}-Butyric Acid Methyl Ester (PCBM). *Phys. Chem. Chem. Phys.* **2016**, *18*, 1185−1190.
(22) Chen, L.; Wang, X.; Kumar, S. Thermal Transport in Fullerene Derivatives Using Molecular Dynamics Simulations. *Sci. Rep.* **2015**, *5*, 12763.
(23) Plimpton, S. Fast Parallel Algorithms for Short-Range Molecular Dynamics. *J. Comput. Phys.* **1995**, *117*, 1−19.
(24) Maple, J. R.; Dinur, U.; Hagler, A. T. Derivation of Force Fields for Molecular Mechanics and Dynamics from *Ab Initio* Energy Surfaces. *Proc. Natl. Acad. Sci. U. S. A.* **1988**, *85*, 5350−5354.
(25) Sun, H. Ab Initio Calculations and Force Field Development for Computer Simulation of Polysilanes. *Macromolecules* **1995**, *28*, 701−712.
(26) Hoppe, H.; Sariciftci, N. S. Morphology of Polymer/Fullerene Bulk Heterojunction Solar Cells. *J. Mater. Chem.* **2006**, *16*, 45−61.
(27) Hoover, W. G. Canonical dynamics: Equilibrium Phase-Space Distributions. *Phys. Rev. A: At., Mol., Opt. Phys.* **1985**, *31*, 1695−1697.
(28) Schelling, P. K.; Phillpot, S. R.; Keblinski, P. Comparison of Atomic-Level Simulation Methods for Computing Thermal Conductivity. *Phys. Rev. B: Condens. Matter Mater. Phys.* **2002**, *65*, 144306.
(29) Sellan, D. P.; Landry, E. S.; Turney, J. E.; McGaughey, A. J. H.; Amon, C. H. Size Effects in Molecular Dynamics Thermal Conductivity Predictions. *Phys. Rev. B: Condens. Matter Mater. Phys.* **2010**, *81*, 214305.
(30) McGaughey, A.; Kaviany, M. Thermal Conductivity Decomposition and Analysis Using Molecular Dynamics Simulations. Part I. Lennard-Jones Argon. *Int. J. Heat Mass Transfer* **2004**, *47*, 1783−1798.
(31) McGaughey, A.; Kaviany, M. Thermal Conductivity Decomposition and Analysis Using Molecular Dynamics Simulations: Part II. Complex Silica Structures. *Int. J. Heat Mass Transfer* **2004**, *47*, 1799−1816.
(32) Ong, W.-L.; O'Brien, E. S.; Dougherty, P. S. M.; Paley, D. W.; Fred Higgs, C., III; McGaughey, A. J. H.; Malen, J. A.; Roy, X. Orientational Order Controls Crystalline and Amorphous Thermal Transport in Superatomic Crystals. *Nat. Mater.* **2016**, *16*, 83−88.
(33) Giri, A.; Braun, J. L.; Hopkins, P. E. Implications of Interfacial Bond Strength on the Spectral Contributions to Thermal Boundary Conductance Across Solid, Liquid, and Gas Interfaces: A Molecular Dynamics Study. *J. Phys. Chem. C* **2016**, *120*, 24847−24856.
(34) Sääskilahti, K.; Oksanen, J.; Linna, R. P.; Tulkki, J. Thermal Conduction and Interface Effects in Nanoscale Fermi-Pasta-Ulam Conductors. *Phys. Rev. E* **2012**, *86*, 031107.
(35) Ong, Z.-Y.; Pop, E. Frequency and Polarization Dependence of Thermal Coupling between Carbon Nanotubes and SiO_2. *J. Appl. Phys.* **2010**, *108*, 103502.
(36) Domingues, G.; Volz, S.; Joulain, K.; Greffet, J.-J. Heat Transfer between Two Nanoparticles through Near Field Interaction. *Phys. Rev. Lett.* **2005**, *94*, 085901.
(37) Allen, M. P.; Tildesley, D. J. *Computer Simulation of Liquids*; Oxford University Press: Oxford U.K., 1989.

DOI: 10.1021/acs.jpclett.7b00609
J. Phys. Chem. Lett. 2017, 8, 2153−2157